Title
Deformation and strength of mantle relevant garnets: Implications for the subduction of basaltic-rich crust

Journal
American Mineralogist, 106(7)

ISSN
0003-004X

Authors
Vennari, Cara E
Lin, Feng
Kunz, Martin
et al.

Publication Date
2021-07-01

DOI
10.2138/am-2021-7587

Word count:

Deformation and Strength of Mantle Relevant Garnets: Implications for the Subduction of Basaltic-rich Crust

Cara E. Vennari[1,2*], Feng Lin[2], Martin Kunz[3], Masaki Akaogi[4], Lowell Miyagi[2], and Quentin Williams[5]

[1]Department of Geophysical Sciences, University of Chicago, Chicago, Illinois 60637, USA.

[2]Geology and Geophysics, University of Utah, Salt Lake City, Utah 84112, USA. [3]Advanced Light Source, Lawrence Berkeley National Laboratory, Berkeley, California 94720, USA.

[4]Department of Chemistry, Gakushuin University, Tokyo, Japan. [5]Earth and Planetary Sciences, University of California Santa Cruz, Santa Cruz, California 95064, USA.

Abstract

Garnet is an important mineral phase in the upper mantle as it is both ~~abundant in normal mantle~~an important component in bulk mantle rocks, and a primary phase ~~within~~ at high-pressure within subducted basalt. Here, we focus on the strength of garnet and the texture that develops within garnet during accommodation of differential deformational strain. We use X-ray diffraction in ~~a~~ radial geometry to analyze texture development in situ in three garnet compositions under pressure at 300 K: a natural garnet ($Py_{67}Alm_{33}$) to 30 GPa, and two synthetic majorite-bearing compositions ($Py_{59}Mj_{41}$ and $Py_{42}Mj_{58}$) to ~~high pressures~~44 GPa. All three garnets develop a modest (100) texture at elevated pressure under axial compression. Elasto-viscoplastic self-consistent (EVPSC) modeling suggests that two slip systems are active in ~~all~~ the three garnet compositions at all pressures studied: {110}<1-11> and {001}<110>. We are able to determine a flow strength of ~5 GPa at pressures between 10 to 15 GPa for all three garnets; these values are higher than previously measured yield strengths measured on natural and majoritic garnets.

Strengths calculated using the experimental lattice strain differ from the strength generated from those calculated using EVPSC. ~~These~~ $Py_{59}Mj_{41}$, $Py_{59}Mj_{41}$ and $Py_{42}Mj_{58}$ ~~garnets~~ are of comparable strength to each other at room temperature, which indicates that majorite substitution does not greatly affect the strength of garnets. Additionally, all three garnets are of similar strength ~~at room temperature to~~ as lower mantle phases such as bridgmanite and ferropericlase, suggesting that garnet~~s~~ ~~are of comparable strength~~may not be notably stronger than the surrounding ~~to~~ lower mantle/deep upper mantle phases at the base of the upper mantle.

Keywords: high-pressure experiment, garnet, texture, strength, radial X-ray diffraction

Introduction

Our understanding of mantle heterogeneity and circulation is largely from observations of discontinuities and anisotropy in seismic wave velocity at depth. The upper mantle's seismic heterogeneity has been explained by a combination of preferred orientation of upper mantle minerals, chemically distinct previously subducted material, phase changes in minerals and partial melting. Small scale heterogeneities have been observed via seismology (e.g., Hedlin et al. 1997), and some of those heterogeneities have been explained as subducted basaltic lithosphere via geochemical and geophysical observations (Davies 1984), and minor seismic reflections (Williams and Revenaugh 2005). By the same token, shape-preferred orientation of (likely basaltic) ~~heterogeneities~~ mantle inclusions has been invoked as one of the possible origins for mantle anisotropy. It has long been appreciated that material of basaltic chemistry is likely a common constituent of the mantle (e.g., Ringwood, 1962); it has been estimated that the upper mantle could contain subducted or delaminated basalt ranging from 5% to 40% (e.g., Allègre & Turcotte, 1986; Cammarano et al., 2009; Hirschmann & Stolper, 1996; Lundstrom et al., 2000;

Schmerr et al., 2013; Williams & Revenaugh, 2005; Xu et al., 2008). The significant seismic anisotropy within the Earth's upper mantle is likely due to the shearing and stretching of heterogeneous assemblages within the mantle, including subducted basaltic slabs and depleted mantle dunite (McNamara et al. 2001). On the microscopic scale, this deformation of mantle rocks can give rise to crystallographic preferred orientation (texture). Direct observations of subducted slab anisotropy are limited due to the lack of ray paths through subducted slabs, and because the mantle wedge and sub-slab anisotropy obscure slab anisotropy~~ due to upper mantle anisotropy~~.~~;~~ ~~nevertheless~~Nevertheless, there have been a few observations of anisotropy within slabs (e.g., Tian and Zhao 2012).

Hence, garnet-dominated lithologies are relevant to the mantle due to their presence in mafic and high-pressure metamorphic assemblages, such as subducted oceanic crust. Our understanding of the strength of garnets under pressure is derived largely from naturally deformed eclogites ~~which~~ where they are resistant to plastic deformation, especially in the presence of weaker minerals like omphacite and quartz that accommodate strain (e.g., Bascou et al. 2001). In low pressure metamorphic facies, garnet is thought to deform via grain boundary sliding rather than intracrystalline deformation (e.g., Zhang & Green 2007). However, in garnet-dominated facies, like at the top of subducted slabs within the transition zone, ~90% of the volume of the crustal material is expected to be majoritic garnet; hence, understanding the deformation of the monomineralic, and especially majorite-bearing, garnet is ~~highly relevant~~important. Garnet has been shown to be strong compared to other mantle materials, indicating that the garnet rich zones (i.e. subducted oceanic crust) may be stronger than the surrounding mantle (Karato et al. 1995).

Garnet has a structure based on a bcc lattice (space group *Ia*3*d*). The garnet structure readily incorporates other chemical elements into its crystal structure; this creates extensive solid solutions and changes the stability field of, for example, majoritic garnets (with the introduction of Al). Work on the deformation of pyropic garnets has been conducted using electron backscatter diffraction on naturally deformed eclogite assemblages. Polycrystal plasticity modeling suggests that the {110 }<1-11> slip system accommodates over 86% of strain resulting in the <100> direction aligning with the compression direction (Mainprice et al. 2004). The dominant Burgers vector for naturally deformed silicate garnets in a range of temperature regimes is ½<1-11>, which most commonly operates on the {110} plane (Voegelé et al. 1998a). This supports the results of an experimental deformation study on almandine rich garnet where the dominant slip systems are ½<111> on {1-10}, {11-2} or {12-3}, or <100> on {010} or {011} (Voegelé et al. 1998b). Other deformation experiments on majorite-pyrope garnets with ex situ transmission electron microscopy analysis indicate Burgers vectors of <100> and ½<111> at high pressures and temperatures (Couvy et al. 2011).

A study on the strength of garnets has been conducted using high-pressure in situ X-ray diffraction in radial geometry on a natural grossular-rich garnet (Kavner 2007); however, while the strength of this garnet was characterized, the resulting textures and deformation mechanism were not investigated. Similarly, the strength of a majoritic garnet was studied within an axial configuration, but also without investigation of slip system activities (Kavner et al. 2000). Hunt et al. (2010) reported that majorite is slightly weaker than pyrope at ~~transition zone~~lithospheric and upper mantle pressures and temperatures. In a comparison of olivine and pyrope, pyrope was observed to be stronger at upper mantle pressures and temperatures~~.~~ (Li et al. 2006). Recently, Girard et al. (~~Girard et al.~~ 2020) reported high temperature and pressure axial deformation on pyrope for use as a stress sensor material in high pressure and temperature experiments. Hence, we study the high-pressure strength and deformation of natural pyrope and synthetic pyrope-majorite garnets and report their active slip systems up to lower mantle pressures using radial diffraction in the diamond anvil cell. Our room temperature measurements provide constraints on the low-temperature strength and slip systems of garnet, and therefore provide a ~~lower bound~~low temperature bound on the rheologic behavior of garnets, while also providing insights into the compositional dependence of deformation mechanisms and strength.

Methods

Experiments were conducted on three garnets: pyrope (UCSC #3248, var. rhodolite, with composition $Py_{67}Alm_{33}$, $(Mg_{0.67}Fe_{0.33})_3Al_2(SiO_3)_4$)) from Franklin, Macon Co., North Carolina (Henderson 1931), $Py_{59}Mj_{41}$ ($Mg_3(Al_{0.59}(MgSi)_{0.41})_2(SiO_3)_4$), and $Py_{42}Mj_{58}$ ($Mg_3(Al_{0.42}(MgSi)_{0.58})_2(SiO_3)_4$). The majorite-bearing samples were synthesized at high pressures, and these aliquots have previously been described and characterized (Akaogi et al. 1987; McMillan et al. 1989). Gold (1-5 wt%) with a grain size of 5.5 – 9.0 μm was used as the pressure standard (Anderson et al. 1989). Pyrope was ground for 1.5 hours with acetone in an agate mortar and pestle, followed by an additional 30 minutes with the gold to ensure even dispersal. $Py_{59}Mj_{41}$ and $Py_{59}Mj_{41}$ were loaded with a flake of gold present in the sample chamber. A BX90 style diamond anvil cell was used for diffraction with a radial geometry at 300 K. Diamonds with culets of 300 μm were used. Gasket material was comprised of a kapton gasket with a boron-epoxy insert (50-80 μm thick and ~350 μm in diameter; Merkel & Yagi, 2005); the sample diameter was 60-80 μm.

Diffraction images were collected at the Advanced Light Source, beamline 12.2.2 (Kunz et al. 2005) using a MAR3450 image plate with X-rays monochromated to 25 keV (wavelength

0.4978 Å) and a sample to detector distance of ~330 mm. Wavelength, sample to detector distance, instrument broadening, peak shape, crystallite size, microstructure and texture were calibrated using the NIST standard CeO_2, and initial fits to the instrument calibrations were completed using DIOPTAS (Prescher and Prakapenka 2015), with refinements completed with the MAUD software (Lutterotti et al. 1997).

Diffraction images were processed using Fit2D (Hammersley 2016) coupled with fit2D2maud: images were unrolled by integrating over 5° azimuthal arcs, for a total of 72 spectra per diffraction image. Rietveld analysis implemented in the MAUD software (Lutterotti et al. 1997) was used to extract texture generally following the procedure for DAC data outlined in Wenk et al. (2014). Textures were calculated using the E-WIMV algorithm within MAUD, with 10° resolution for the orientation distribution function, with fiber symmetry imposed. Pole figures and inverse pole figures were smoothed and produced using BEARTEX (Wenk et al. 1998).

Lattice strain and texture development are modeled together using the elasto-viscoplastic self-consistent method (EVPSC) (Wang et al. 2010). EVPSC is an effective medium method, which treats single grains in an aggregate as inclusions in a homogeneous but anisotropic medium. Plastic strain rate is described by a rate-sensitive constitutive law for each slip system. The properties of the medium are determined by the average of all the inclusions. At each deformation step, the inclusions interact with the medium and the medium is updated when the average strain and stress of all inclusions equal the macroscopic stress and strain. The plastic behavior of the inclusion at the local level is described by a non-linear rate-sensitive constitutive law of varying slip systems:

$$\dot{\varepsilon}_{ij}=\dot{\gamma}_0 \sum_s m_{ij}^s \left\{ \frac{\left| m_{kl}^s \sigma_{kl} \right|}{\tau^s} \right\}^n sgn\left(m_{kl}^s \sigma_{kl} \right) \qquad (1)$$

$$\dot{\varepsilon}_{ij}=\dot{\gamma}_0 \sum_s m_{ij}^s \left\{ \frac{\left| m_{kl}^s \sigma_{kl} \right|}{\tau^s} \right\}^n sgn\left(m_{kl}^s \sigma_{kl} \right)$$

Where $\dot{\varepsilon}_{ij}$ is the strain rate tensor, $\dot{\gamma}_0$ is the reference shear strain rate, τ^s is the critical resolved shear stress (CRSS) value of a slip system *s* at the reference strain rate, which controls the slip system activation. m_{kl}^s is the symmetric Schmid factor for the slip system *s*, *n* is an empirical stress exponent, and σ_{kl} is the local stress tensor. When the stress resolved onto a given slip system is close to the threshold value τ^s, deformation will occur on the slip system.

Since pressure and strain increase simultaneously in DAC experiments, it is not possible to separate the pressure and strain hardening effects on CRSS. They are both included in the pressure dependence of the CRSS. In this study, $\tau^s = \tau_0^s + d\tau / dP \cdot P + d^2 \tau / d P^2 \cdot P^2$, where τ_0^s is the initial CRSS and $d\tau / dP$ and $d^2 \tau / d P^2$ are the first and second order pressure dependence of CRSS. In order to simulate high pressure experimental data, a pressure dependence of the elastic moduli was used. The details for using EVPSC to simulate high pressure data can be found in Lin et al. (2017).

Results and Discussion

Differential Stress and Elasticity

X-ray diffraction data were collected on $Py_{67}Alm_{33}$ up to 31 GPa, and on $Py_{59}Mj_{41}$ and $Py_{42}Mj_{58}$ up to 44 GPa. Representative experimental and calculated diffraction images are shown in Fig. S1 at 31 or 32 GPa, depending on the sample. Overall, the peaks broaden as pressure is increased; this is due to microstrain (defect structure and strain heterogeneity) within the lattice and likely grain size reduction. Using the four diffraction lines (400), (420), (640) and (321), which are strong and do not overlap (1) with other diffraction lines for garnet or (2) with the gold pressure standard, we are able to measure accurate values of lattice strain ($Q(hkl)$); see Text S1 and Fig. S1. The Q-values for these four lines increase at similar rates up to the highest pressures probed (Fig. 1).

Texture and Plasticity

With increasing pressure, modest texturing (plastic deformation) is observed as demonstrated by the development of intensity variations along the Debye rings. As pressure is increased, a (100) maximum develops in the compression direction for all three compositions of garnet. On compression to 30 GPa, the pole density increases to a maximum of ~1.5 times a random distribution (m.r.d: multiples of random distribution), with a minimum of ~0.80 m.r.d. in (111) (Fig. 2) in $Py_{67}Alm_{33}$. $Py_{59}Mj_{41}$ and $Py_{42}Mj_{58}$ also have a maximum of m.r.d. at (100) at 32 GPa ($Py_{59}Mj_{41}$ and $Py_{42}Mj_{58}$ respectively). The (100) texture remains up to the highest pressures probed for both $Py_{59}Mj_{41}$ and $Py_{42}Mj_{58}$ (Fig. 2). Interestingly, we do not see a difference in texture with crystal chemistry; Voegelé et al. (1998a) also reported that even across a wide range of chemistry, similar deformation mechanisms were observed in silicate garnets.

The (100) normal aligning at high angles to the compression direction has been observed in other garnets by Mainprice et al. (2004); however, they also found that there was a maximum of (110) poles in the compression direction. These differences indicate that the slip systems described by Mainprice et al. (2004) may not be sufficient to fully model the texture we observe. The pole figure densities (m.r.d.) are low compared to other mantle materials at similar pressures (e.g., MgO and bridgmanite; Merkel, 2002). This has been attributed to the large number (66) of possible slip systems within the garnet structure or a change in deformation mechanism to diffusion creep (Mainprice et al. 2004). In our experiments at room temperature, the low m.r.d.

values are most likely due to the high number of symmetric variants for slip systems and relatively low strain (~20%). The previous *in situ* study of strength of grossular garnet alluded to possible plastic deformation, but did not characterize textures of deformation mechanisms (Kavner 2007).

EVPSC Modeling and Comparison to Experimental Results

We modeled the evolution of ~~Texture~~ texture and lattice strain ~~evolution was modeled~~ as a function of slip system activities using the EVPSC code (Wang et al. 2010). This code is advantageous because it can account for both the elastic and the viscoplastic behavior of the material by modeling lattice strain coupled with grain rotation from dislocation glide rather than only using either the elastic (e.g. Elastic Plastic Self-Consistent method, EPSC; Turner & Toivi, 2000) or the viscoplastic (Viscoplastic Self-Consistent method, VPSC; ~~Lebensohn & Tomé, 1994).~~

With EVPSC, we tested seven slip systems ~~were tested~~: {110}<1-11>, {112}<11-1>, {123}<11-1>, {001}<110>, {011}<100>, {010}<100>, and {110}<1-10>. Lebensohn & Tomé, 1994). We imposed a strain rate of $1 * 10^{-4}$ s^{-1} as estimated by Marquardt and Miyagi (2015) for a total strain of ~22%. We used the shear modulus reported in Sinogeikin and Bass (2000). Based on the *Q*(*hkl*) of (400), (420), (640), and (642) and the texture development with pressure, no single slip system can explain the deformation of pyrope at high pressures (Fig. S2). Only with the activation of two of these slip systems ({110}<1-11> and {001}<110>; Fig. 3**,** Table S1) can we generate the observed textures and lattice strain development in all three garnets. The experimental *Q(hkl)* values and texture are in excellent agreement with the EVPSC modeling (Fig. 3).

Elasticity

In order to compare our results with previous results for other garnets and mantle phases, we use the Voigt approximation for the uniaxial stress component,

$$t=6G<Q(hkl)>(¿\sigma_3-\sigma_1=\sigma_Y) \quad (2)$$

$$t=6G<Q(hkl)>(¿\sigma_3-\sigma_1=\sigma_Y)$$

$$t=6G<Q(hkl)>(¿\sigma_3-\sigma_1=\sigma_Y)$$

where *t* is the uniaxial stress component, *G* is the shear modulus, and *Q*(*hkl*) is the lattice strain. With this, we are able to estimate the flow strength and measure the elastic limit of the three garnets. We utilize a shear modulus of 94.7 GPa and its pressure derivative d*G*/*dP* of 1.76 from Chai et al. (1997) for $Py_{67}Alm_{33}$ and a shear modulus of 90 GPa and its pressure derivative of 1.3 for both $Py_{59}Mj_{41}$ and $Py_{42}Mj_{58}$ (Sinogeikin and Bass 2002). We find that all three garnets have a flow stress of ~5.5 GPa (Fig. 4, Table S2) using this approximation.

In comparing the relative strengths of these garnets, it is apparent that changes to the X and Y cations (where the standard chemistry is $X_3Y_2(SiO_3)_4$) in these samples have relatively minor effects on the elastic limit of garnet, at least in terms of Mg vs. Fe substitution into the X site and Al vs. Mg and Si substitution into the Y site. The strengths of these garnets are also comparable to those of other mantle phases (Fig. 4). In all the studies we compared, the deformation was imposed using a diamond anvil cell at room temperature. These garnets having equivalent strengths at 300 K is in accord with the relative strength measurements of Hunt et al. (2010). Bridgmanite has a comparable flow strength and can accommodate similar differential stress levels up to ~20 GPa (Merkel et al., 2003). End-member periclase is stronger than garnet at all pressures probed (Merkel, 2002). We find that pyrope is stronger than grossular garnet, as reported by Kavner (2007). We have four possible explanations for this difference in strength: (1) There could be grain size differences between this study and ~~hers~~the Kavner (2007) study; (2) there may be an intrinsic strength difference associated with Ca substitution in the X site of the garnet crystal structure; (3) there may be a higher water content/defect concentration in the grossular samples; and/or (4) the azimuthal coverage may not have allowed for full characterization of the strength of the grossular garnet. With respect to this final explanation, we note that we probe from 0-360º with 5º arcs, while Kavner (2007) utilized 8 discrete angles spanning 180º and fit *Q*-values from those angles.

The experimental strength values approximated using equation (2) and those calculated ~~strength values~~using EVPSC (Fig. 4) are in excellent agreement up to ~~~12~~ 10 GPa, and in ~~good~~ modest agreement up until the highest pressures probed. The ~~slight~~ divergence at high pressures is common in high pressure deformation experiments (e.g., Burnley & Zhang, 2008). ~~There is no clear trend of *Q(hkl)* causing a deviation at higher pressures (Fig. S3), although~~ Although all four of the *Q(hkl)* analyzed in this study were systematically higher than the modeled strength, there is no clear trend of which *Q(hkl)* causes the deviation at higher pressures (Fig. S3).

A limitation of diffraction-based strength studies is that they are limited by those planes satisfying the diffraction condition. As such, we are unable to measure the lattice strain of all planes within our samples, so we are inherently limiting the input for the approximation using equation (2). By using the strength calculated with EVPSC (Fig. 4), a Reuss boundary condition is not imposed on the data, and we are calculating~~ed~~ the true stress. This ~~is~~ difference in calculated strength is demonstrated by our discrepancy in the experimental and modeled strengths above ~10 GPa, and ~18% at 44 GPa. Our results support the assertion from Burnley & Zhang (2008) that strengths generated only with experimental lattice strain are not a good proxy for the macroscopic stress of the system Burnley & Zhang (2008). Hence, we caution against using garnet as a macroscopic stress sensor at least above the flow strength as suggested by Girard et al. (2020).

Comparison with Previously Observed Slip Systems in Garnets

The two slip systems that are active in $Py_{67}Alm_{33}$, $Py_{59}Mj_{41}$, and $Py_{42}Mj_{58}$ at high pressures have been observed in *ex situ* analysis of deformed garnets with the two most common Burgers vectors being <110> and ½<1-11>. For example, eclogite garnets deform such that the (100) normal aligns with the compression direction and slip occurs on the {110}<1-11> system (Mainprice et al. 2004). Over our experimental pressure range, the majority (~60-64%) of the strain in pyrope is accommodated by this slip system. This Burgers vector is also consistent with the slip observed by (Voegelé et al. 1998b) in $Py_{20}Alm_{73}Sp_2Gr_5$ on ½<111> and by Couvy et al. (2011) in $Py_{30}Mj_{70}$. While Voegelé et al. (1998b) reported equivalent slip in the ½<1-11> direction on the {110}, {112}, and {123} planes, Mainprice et al. (2004) reported 86% of the slip in garnets in naturally deformed eclogites occurs via the {110}<1-11> slip system. Here, we note that it is difficult to distinguish between the three slip planes {110}, {112}, and {123} due to the similarity of their textures and development of *Q*-values. Our selection of the {110} plane is partially constrained from the observation from Mainprice et al. (2004). Notably, the {110}<1-11> system appears to be active in non-silicate garnets at ambient pressure at least up to temperatures that correspond to ~0.84 of their melting temperature (Karato et al. 1994). Therefore, it appears likely that our 300 K deformation experiments access the same primary slip system as is present at high temperatures in other garnets.

The other ~40% of the strain is accommodated via the {001}<110> system. This slip system has not been observed in garnets in high pressure/temperature deformation experiments

(Voegelé et al. 1998b), nor in most deformed eclogites (Mainprice et al. 2004). However, the resulting texture has been observed in other cubic materials. For example, this slip system has been observed in ferropericlase at high pressures and temperatures (Immoor et al. 2018) and is common in halite (Wenk et al. 1989).

Differences between the secondary slip system of this experiment and observations in garnets probed via TEM could be partially due to the difference in temperature between the high temperatures that the garnets experienced during either the experiments or metamorphism, and our 300 K experiments. Garnets analyzed in Mainprice et al. (2004) experienced pressures over 2.1 GPa and temperatures ranging from 480 ºC to >700 ºC. If this is the case, {110}<1-11> deformation may soften under temperature relative to the {001}<110> system. Indeed, it is well known that slip system activities can change with temperature, as for example in ferropericlase (Heidelbach et al. 2003; Immoor et al. 2018). Alternatively, the secondary slip system may result from the higher pressures probed in this study compared to the TEM studies: ferropericlase, for example, activates different slip systems below 20-30 GPa and above 60 GPa (Amodeo et al. 2012; Marquardt and Miyagi 2015).

Seismic Signature

Shear wave splitting can be generated by the combination of single crystal elastic anisotropy and texturing. Brillouin spectroscopic studies of garnets have demonstrated that they remain close to elastically isotropic to high pressures. The anisotropy factor of pyrope ($2*C_{44}/(C_{11}-C_{12}) - 1$) was observed to be -0.02 at ambient conditions, and 0.01 at 14 GPa (Sinogeikin and Bass 2000). With a linear extrapolation to 30 GPa, the anisotropy would be 0.04. P- and S- wave velocities were calculated at 30 GPa with simple shear applied (100% shear strain), and using the extrapolated elastic constants from Sinogeikin and Bass [2000] and the observed texture in

$Py_{67}Alm_{33}$ (Fig. S4). Overall, the S-wave shear splitting of a polycrystalline aggregate has a maximum of 0.28% in the (100) direction. Since the shear splitting of a rock assemblage depends on each material's contribution to the shear splitting, we expect that pyropic garnet (or, by extension, similarly deforming majoritic garnets) does not play a role in anisotropy in slabs in the upper mantle. Overall, seismic anisotropy observed in subducted slabs is likely not due to cubic solid solutions that are similar to the cubic $Py_{67}Alm_{33}$, $Py_{59}Mj_{41}$, and $Py_{42}Mj_{58}$ garnets that we have characterized. However, ~~end-member tetragonal majorite (e.g., Pacalo & Weidner, 1997) and~~ andradite (Jiang et al. 2004) and end-member tetragonal majorite (e.g., Pacalo & Weidner, 1997) garnets are less isotropic, and could represent slight contributors to seismic anisotropy in the upper mantle. Nevertheless, a garnet-dominated crust of formerly basaltic chemistry is likely an isotropic cap on top of anisotropic, $(Mg,Fe)_2SiO_4$-dominated former oceanic lithosphere.

Conclusions

We provide the first *in situ* analysis of the plastic deformation and flow strength of mantle relevant $Py_{67}Alm_{33}$ garnet to 30 GPa and $Py_{59}Mj_{41}$, and $Py_{42}Mj_{58}$ to 44 GPa at 300 K. Overall, we have demonstrated that garnet is relatively strong in comparison to other mantle phases. All three garnet compositions exhibit a flow strength~~,~~ of 5.5 GPa at 8 GPa~~, and they can accommodate >6 GPa differential stress above 15 GPa~~ at 300 K, using both equation (2) and with the EVPSC results. This differs markedly from the previously reported strength of grossular garnet (Kavner 2007), and we attribute the differences to either a strong chemical dependency of garnet strength, variations in grain size, different defect contents, or a difference in data coverage; the similar strengths are in agreement with Hunt et al. (2010). Using the elasto-visco plastic self-consistent method, we identify two active slip systems: {110}<1-11> and {001}<110>. Both slip systems are needed to simultaneously match the observed lattice strain and texture development. Slip systems obtained in this study are consistent with previous ex situ analysis of deformed garnets.

Implications

These ambient temperature experiments imply that garnet-rich crustal layers on subducted slabs likely initially behave as comparatively rigid layers compared to ~~in~~ the olivine-dominated upper mantle (particularly if the crustal layer remains relatively cold at depth). The situation within the transition zone and at the top of the lower mantle is more ambiguous, however: both bridgmanite and periclase have strengths that generally are comparable to those that we have measured for this sequence of garnets. Similarly, ringwoodite (Kavner & Duffy, 2001) and wadsleyite (Mosenfelder et al., 2000) each have strengths that seem to be similar to those of garnet at deep transition zone conditions, as well. Accordingly, garnet-enriched regions (possibly derived from basaltic protoliths) may not generate notably rheologically strong layers at the top of the lower mantle or within the deep transition zone, unless they remain colder than the surrounding mantle.

Acknowledgments

We would like to thank Jinyuan Yan for help in preparation of the gaskets and Sam Couper for useful conversations. We would like to thank the following funding sources: US NSF (EAR-1620423, EAR-1654687, EAR PF-1855336). Additional support from the US Department of Energy, National Nuclear Security Administration, through the Capital-DOE Alliance Center (DE-NA0003858). This research used resources of the Advanced Light Source (beamline 12.2.2) at Lawrence Berkeley National Laboratory which is DOE Office of Science User facility under Contract No. DE-AC02-05CH11231. This research was partially supported by COMPRES, the Consortium for Materials Properties Research in Earth Sciences under NSF Cooperative Agreement EAR 1606856.

References

Akaogi, M., Navrotsky, A., Yagi, T., & Akimoto, S. (1987). Pyroxene-garnet transformation: Thermochemistry and elasticity of garnet solid solutions, and application to a pyrolite mantle. In Y. E. Manghnani, M.H. and Syono (Ed.), *High Pressure Research in Mineral Physics* (pp. 251–260). Washington, D.C.

Allègre, C. J., & Turcotte, D. L. (1986). Implications of a two-component marble-cake mantle. *Nature*, *323*(6084), 123–127. https://doi.org/10.1038/323123a0

Amodeo, J., Carrez, P., & Cordier, P. (2012). Modelling the effect of pressure on the critical shear stress of MgO single crystals. *Philosophical Magazine*, *92*(12), 1523–1541. https://doi.org/10.1080/14786435.2011.652689

Anderson, O. L., Isaak, D. G., & Yamamoto, S. (1989). Anharmonicity and the equation of state for gold. *Journal of Applied Physics*, *65*(4), 1534–1543. https://doi.org/10.1063/1.342969

Bascou, J., Barruol, G., Vauchez, A., Mainprice, D., & Egydio-Silva, M. (2001). EBSD-measured lattice-preferred orientations and seismic properties of eclogites. *Tectonophysics*, *342*(1–2), 61–80. https://doi.org/10.1016/S0040-1951(01)00156-1

Burnley, P. C., & Zhang, D. (2008). Interpreting in situ x-ray diffraction data from high pressure deformation experiments using elastic-plastic self-consistent models: An example using quartz. *Journal of Physics Condensed Matter*, *20*(28). https://doi.org/10.1088/0953-8984/20/28/285201

Cammarano, F., Romanowicz, B., Stixrude, L., Lithgow-Bertelloni, C., & Xu, W. (2009). Inferring the thermochemical structure of the upper mantle from seismic data. *Geophysical*

Journal International, *179*(2), 1169–1185. https://doi.org/10.1111/j.1365-246X.2009.04338.x

Chai, M., Brown, J. M., & Slutsky, L. J. (1997). The elastic constants of a pyrope-grossular-almandine garnet to 20 GPa. *Geophysical Research Letters*, *24*(5), 523. https://doi.org/10.1029/97GL00371

Couvy, H., Cordier, P., & Chen, J. (2011). Dislocation microstructures in majorite garnet experimentally deformed in the multi-anvil apparatus. *American Mineralogist*, *96*(4), 549–552. https://doi.org/10.2138/am.2011.3671

Davies, G. F. (1984). Geophysical and isotopic constraints on mantle convection: An interim synthesis. *Journal of Geophysical Research*, *89*(B7), 6017–6040.

Hammersley, A. P. (2016). FIT2D: A multi-purpose data reduction, analysis and visualization program. *Journal of Applied Crystallography*, *49*, 646–652. https://doi.org/10.1107/S1600576716000455

Hedlin, M. A. H., Shearer, P. M., & Earle, P. S. (1997). Seismic evidence for small-scale heterogeneity throughout the Earth's mantle. *Nature*, *287*, 145–150. https://doi.org/10.1038/387145a0

Heidelbach, F., Stretton, I., Langenhorst, F., & Mackwell, S. (2003). Fabric evolution during high shear strain deformation of magnesiowüstite ($Mg_{0.8}Fe_{0.2}O$). *Journal of Geophysical Research: Solid Earth*, *108*(B3). https://doi.org/10.1029/2001jb001632

Henderson, E. P. (1931). Notes on some minerals from the rhodolite quarry near Franklin, North Carolina. *American Mineralogist*, *16*, 563–568.

Hirschmann, M. M., & Stolper, E. M. (1996). A possible role for garnet pyroxenite in the origin of the "garnet signature" in MORB. *Contributions to Mineralogy and Petrology*, *124*(2), 185–208. https://doi.org/10.1007/s004100050184

Hunt, S. A., Dobson, D. P., Li, L., Weidner, D. J., & Brodholt, J. P. (2010). Relative strength of the pyrope-majorite solid solution and the flow-law of majorite containing garnets. *Physics of the Earth and Planetary Interiors*, 87/95.

Immoor, J., Marquardt, H., Miyagi, L., Lin, F., Speziale, S., Merkel, S., et al. (2018). Evidence for {100}<011> slip in ferropericlase in Earth's lower mantle from high-pressure/high-temperature experiments. *Earth and Planetary Science Letters*, *489*, 251–257. https://doi.org/10.1016/j.epsl.2018.02.045

Jiang, F., Speziale, S., Shieh, S. R., & Duffy, T. S. (2004). Single-crystal elasticity of andradite garnet to 11 GPa. *Journal of Physics: Condensed Matter*, *16*, S1041–S1052. https://doi.org/10.1088/0953-8984/16/14/014

Karato, S., Wang, Z., & Fujino, K. (1994). High-temperature creep of yttrium-aluminum garnet single crystals. *Journal of Materials Science*, *29*, 6458–6462.

Karato, S., Wang, Z., Liu, B., & Fujino, K. (1995). Plastic deformation of garnets: systematics and implications for the rheology of the mantle transition zone. *Earth and Planetary Science Letters*, *130*(1–4), 13–30. https://doi.org/10.1016/0012-821X(94)00255-W

Kavner, Abby. & Duffy, T. S. (2001). Strength and elastictiy of ringwoodite at upper mantle pressures. *Geophysical Research Letters*, *28*(14), 2691–2694. https://doi.org/doi/10.1029/2000GL012671

Kavner, Abby. (2007). Garnet yield strength at high pressures and implications for upper mantle and transition zone rheology. *Journal of Geophysical Research*, *112*(B12), 1–9. https://doi.org/10.1029/2007JB004931

Kavner, Abby, Sinogeikin, S. V, Jeanloz, R., & Bass, J. D. (2000). Equation of state and strength of natural majorite. *Journal of Geophysical Research: Solid Earth*, *105*(B3), 5963–5971. https://doi.org/10.1029/1999JB900374

Kunz, M., MacDowell, A. A., Caldwell, W. A., Cambie, D., Celestre, R. S., Domning, E. E., et al. (2005). A beamline for high-pressure studies at the Advanced Light Source with a superconducting bending magnet as the source. *Journal of Synchrotron Radiation*, *12*(5), 650–658. https://doi.org/10.1107/S0909049505020959

Lebensohn, R. A., & Tomé, C. N. (1994). A self-consistent viscoplastic model: prediction of rolling textures of anisotropic polycrystals. *Materials Science and Engineering A*, *175*(1–2), 71–82. https://doi.org/10.1016/0921-5093(94)91047-2

Li, L., Long, H., Raterron, P., & Weidner, D. (2006). Plastic flow of pyrope at mantle pressure and temperature. *American Mineralogist*, *91*(4), 517–525. https://doi.org/10.2138/am.2006.1913

Lin, F., Hilairet, N., Raterron, P., Addad, A., Immoor, J., Marquardt, H., et al. (2017). Elasto-viscoplastic self consistent modeling of the ambient temperature plastic behavior of periclase deformed up to 5.4 GPa. *Journal of Applied Physics*, *122*(20). https://doi.org/10.1063/1.4999951

Lundstrom, C. C., Gill, J., & Williams, Q. (2000). A geochemically consistent hypothesis for MORB generation. *Chemical Geology*, *162*(2), 105–126. https://doi.org/10.1016/S0009-2541(99)00122-9

Lutterotti, L., Matthies, S., Wenk, H.-R., Schultz, A. S., & Richardson, J. W. (1997). Combined texture and structure analysis of deformed limestone from time-of-flight neutron diffraction spectra. *Journal of Applied Physics*, *81*(2), 594–600. https://doi.org/10.1063/1.364220

Mainprice, D., Bascou, J., Cordier, P., & Tommasi, A. (2004). Crystal preferred orientations of garnets: Comparison between numerical simulation and electron back-scattered diffraction (EBSD) measurements in naturally deformed eclogites. *Journal of Structural Geology*, *26*(11), 2089–2102. https://doi.org/10.1016/j.jsg.2004.04.008

Marquardt, H., & Miyagi, L. (2015). Slab stagnation in the shallow lower mantle linked to an increase in mantle viscosity. *Nature Geoscience*, *8*(4), 311–314. https://doi.org/10.1038/ngeo2393

McMillan, P., Akaogi, M., Ohtani, E., Williams, Q., Nieman, R., & Sato, R. (1989). Cation disorder in garnets along the $Mg_3Al_2Si_3O_{12}$-$Mg_4Si_4O_{12}$ join: An infrared, Raman and NMR study. *Physics and Chemistry of Minerals*, *16*, 428–435. https://doi.org/10.1145/3267242.3267259

McNamara, A. K., Karato, S.-I., & van Keken, P. E. (2001). Localization of dislocation creep in the lower mantle: Implications for the origin of seismic anisotropy. *Earth and Planetary Science Letters*, *191*(1–2), 85–99. https://doi.org/10.1016/S0012-821X(01)00405-8

Merkel, S. (2002). Deformation of polycrystalline MgO at pressures of the lower mantle. *Journal of Geophysical Research*, *107*(B11), 2271. https://doi.org/10.1029/2001JB000920

Merkel, S., & Yagi, T. (2005). X-ray transparent gasket for diamond anvil cell high pressure experiments. *Review of Scientific Instruments*, *76*(4), 0–3. https://doi.org/10.1063/1.1884195

Merkel, S., Wenk, H.-R., Badro, J., Montagnac, G., Gillet, P., Mao, H. K., & Hemley, R. J. (2003). Deformation of $(Mg_{0.9},Fe_{0.1})SiO_3$ perovskite aggregates up to 32 GPa. *Earth and Planetary Science Letters*, *209*(3–4), 351–360. https://doi.org/10.1016/S0012-821X(03)00098-0

Pacalo, R. E. G., & Weidner, D. J. (1997). Elasticity of majorite, $MgSiO_3$ tetragonal garnet.

Physics of the Earth and Planetary Interiors, *99*(1–2), 145–154. https://doi.org/10.1016/S0031-9201(96)03158-5

Prescher, C., & Prakapenka, V. B. (2015). *DIOPTAS*: a program for reduction of two-dimensional X-ray diffraction data and data exploration. *High Pressure Research*, (August), 1–8. https://doi.org/10.1080/08957959.2015.1059835

Ringwood, A. E. (1962). A model for the upper mantle. *Journal of Geophysical Research*, *67*(2), 857–867. https://doi.org/10.1029/JZ067i002p00857

Schmerr, N. C., Kelly, B. M., & Thorne, M. S. (2013). Broadband array observations of the 300 km seismic discontinuity. *Geophysical Research Letters*, *40*(5), 841–846. https://doi.org/10.1002/grl.50257

Singh, A K, Balasingh, C., Mao, H., Hemley, R. J., & Shu, J. (1998). Analysis of lattice strain measured under nonhydrostatic pressure. *Journal of Applied Physics*, *83*(12), 7567–7575.

Singh, Anil K., & Balasingh, C. (1993). The lattice strains in a specimen (cubic system) compressed nonhydrostatically in an opposed anvil high pressure setup. *Journal of Applied Physics*, *73*, 4278–4286. https://doi.org/10.1063/1.355786

Singh, Anil K., & Balasingh, C. (1994). The lattice strains in a specimen (hexagonal system) compressed nonhydrostatically in an opposed anvil high pressure setup. *Journal of Applied Physics*, *75*(10), 4956–4962. https://doi.org/10.1063/1.355786

Sinogeikin, S. V., & Bass, J. D. (2000). Single-crystal elasticity of pyrope and MgO to 20 GPa by Brillouin scattering in the diamond cell. *Physics of the Earth and Planetary Interiors*, *120*(1), 43–62. https://doi.org/10.1016/S0031-9201(00)00143-6

Sinogeikin, S. V, & Bass, J. D. (2002). Elasticity of majorite and a majorite-pyrope solid solution to high pressure: Implications for the transition zone. *Geophysical Research Letters*, *29*(2),

1017. https://doi.org/10.1029/2001GL013937

Tian, Y., & Zhao, D. (2012). Seismic anisotropy and heterogeneity in the Alaska subduction zone. *Geophysical Journal International*, *190*(1), 629–649. https://doi.org/10.1111/j.1365-246X.2012.05512.x

Turner, P. A., & Tomé, C. N. (1994). A study of residual stresses in Zircaloy-2 with rod texture. *Acta Metallurgica et Metallica*, *42*(12), 4143–4153.

Voegelé, V., Cordier, P., Sautter, V., Sharp, T. G., Lardeaux, J. M., & Marques, F. O. (1998). Plastic deformation of silicate garnets. II. Deformation microstructures in natural samples. *Physics of the Earth and Planetary Interiors*, *108*(4), 319–338. https://doi.org/10.1016/S0031-9201(98)00111-3

Voegelé, V., Ando, J. I., Cordier, P., & Liebermann, R. C. (1998). Plastic deformation of silicate garnets I. High-pressure experiments. *Physics of the Earth and Planetary Interiors*, *108*, 305–318.

Wang, H., Wu, P. D., Tomé, C. N., & Huang, Y. (2010). A finite strain elastic-viscoplastic self-consistent model for polycrystalline materials. *Journal of the Mechanics and Physics of Solids*, *58*(4), 594–612. https://doi.org/10.1016/j.jmps.2010.01.004

Wenk, H.-R., Canova, G., Molinari, A., & Mecking, H. (1989). Texture development in halite: Comparison of Taylor model and self-consistent theory. *Acta Metallurgica*, *37*(7), 2017–2029. https://doi.org/10.1016/0001-6160(89)90086-2

Wenk, H.-R., Lutterotti, L., Kaercher, P., Kanitpanyacharoen, W., Miyagi, L., & Vasin, R. (2014). Rietveld texture analysis from synchrotron diffraction images. II. Complex multiphase materials and diamond anvil cell experiments. *Powder Diffraction*, *29*(03), 220–232. https://doi.org/10.1017/S0885715614000360

Wenk, H. R., Matthies, S., Donovan, J., & Chateigner, D. (1998). BEARTEX: A Windows-based program system for quantitative texture analysis. *Journal of Applied Crystallography*, *31*(2), 262–269. https://doi.org/10.1107/S002188989700811X

Williams, Q., & Revenaugh, J. (2005). Ancient subduction, mantle eclogite, and the 300 km seismic discontinuity. *Geology*, *33*(1), 1–4. https://doi.org/10.1130/G20968.1

Xu, W., Lithgow-Bertelloni, C., Stixrude, L., & Ritsema, J. (2008). The effect of bulk composition and temperature on mantle seismic structure. *Earth and Planetary Science Letters*, *275*, 70–79. https://doi.org/10.1016/j.epsl.2008.08.012

Zhang, J., & Green, H. W. (2007). Experimental investigation of eclogite rheology and its fabrics at high temperature and pressure. *Journal of Metamorphic Geology*, *25*(2), 97–115. https://doi.org/10.1111/j.1525-1314.2006.00684.x

Fig 1

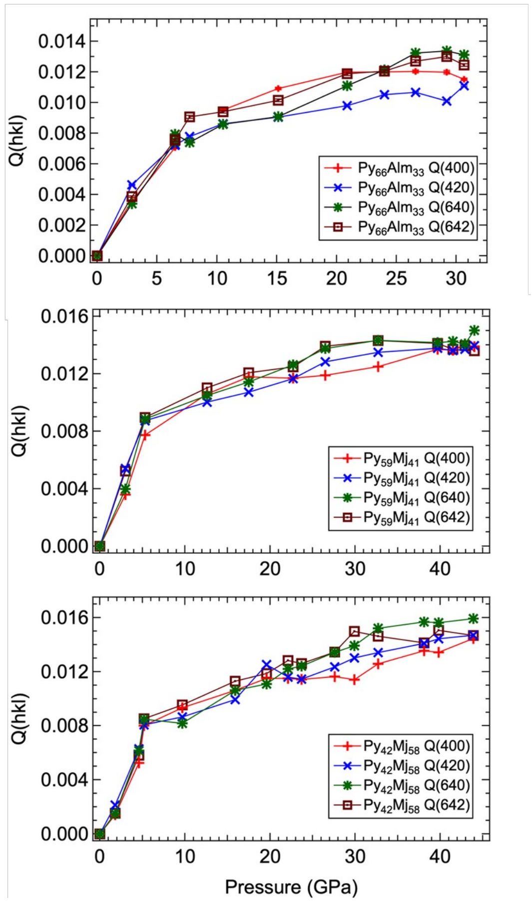

Figure 1. (left) *Q*(*hkl*) with increased pressure of the (400), (420), (640), and (642) diffraction lines for (top) $Py_{67}Alm_{33}$, (middle) $Py_{59}Mj_{41}$, and (bottom) $Py_{42}Mj_{58}$.

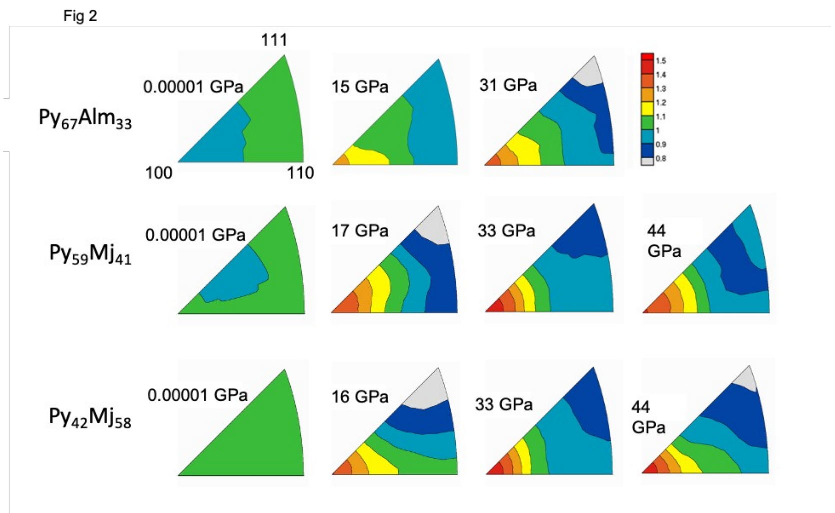

Figure 2. Representative inverse pole figures of $Py_{67}Alm_{33}$, $Py_{59}Mj_{41}$, and $Py_{42}Mj_{58}$ at ambient pressure, ~16 GPa, ~31 GPa and 44 GPa.

Fig 3

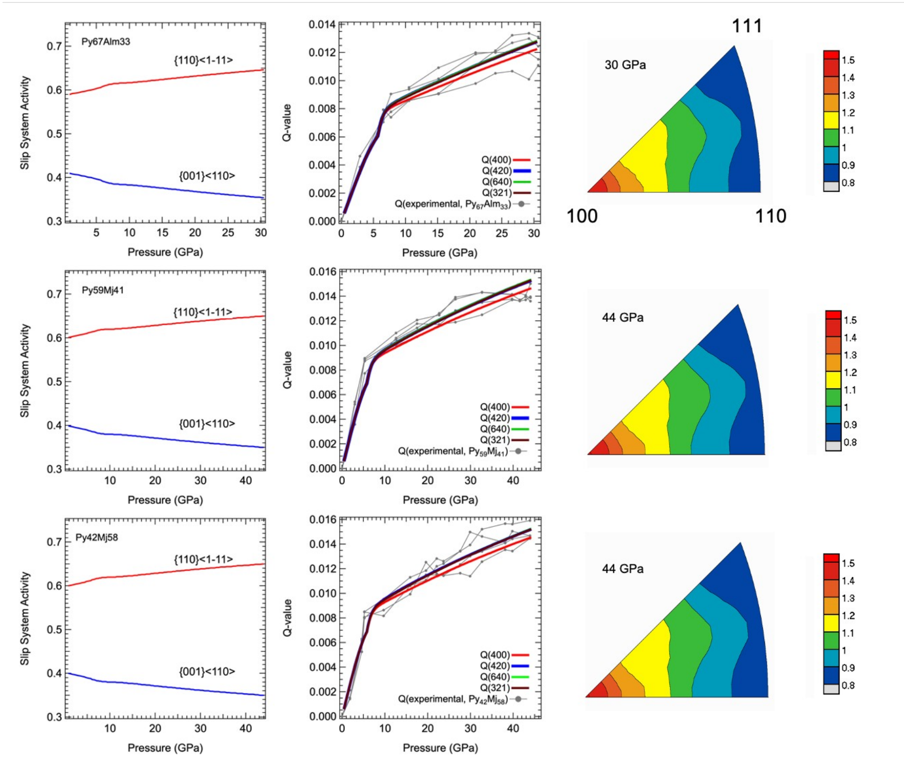

Figure 3. (left) ~~Active~~ Relative activity of slip systems with pressure; (middle) resulting *Q*-factors from active slip systems with pressure compared to experimental *Q*-factors; and (right) synthetic texture at highest pressures probed for (top) $Py_{67}Alm_{33}$, (middle) $Py_{59}Mj_{41}$, (bottom) $Py_{42}Mj_{58}$.

Fig 4

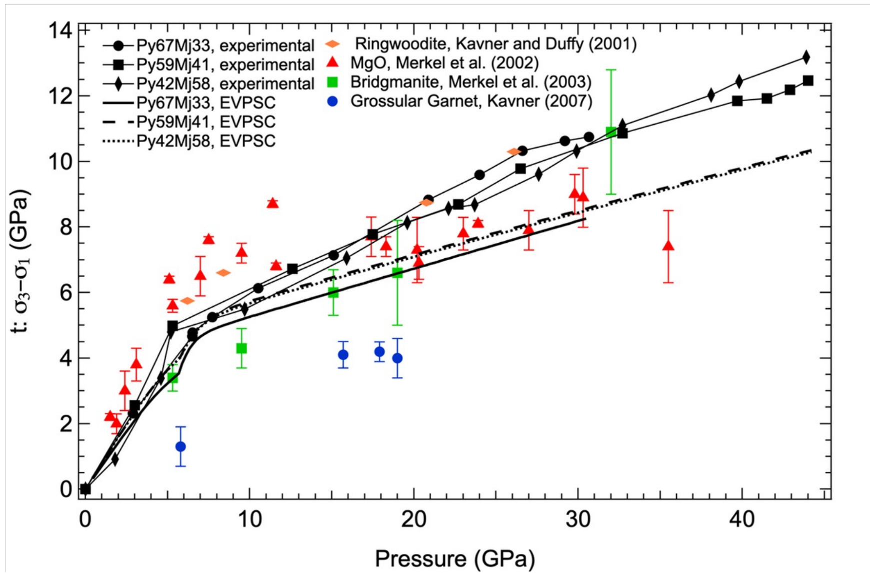

Figure 4. A comparison between the strength as calculated with $t=6G<Q(hkl)>$,EVPSC modeling, and other relevant mantle phases: bridgmanite (Merkel et al. 2003), MgO (Merkel 2002), grossular garnet (Kavner 2007), and ringwoodite (Kavner and Duffy 2001). Error bars for this study are smaller than the symbols.